Electronic Supporting Information

Photothermal in motion: effect of low intensity irradiation on the thermal motion of organic nanoparticles

Moreno Guernelli,[a] *Evangelos Bakalis,*[a] *Alexandra Mavridi-Printezi,*[a] *Vasilis Petropoulos,*[b] *Giulio Cerullo,*[b] *Francesco Zerbetto*[a]* *and Marco Montalti*[a]*

a) Department of Chemistry "Giacomo Ciamician", University of Bologna, Via Selmi 2, 40126 Bologna, Italy

b) Department of Physics, Politecnico di Milano, Piazza L.da Vinci 32, 20133, Milano, Italy

1. Materials and methods

1.1 Materials

All reagents, solvents and chemicals were purchased from Sigma-Aldrich and used without modification, unless otherwise stated.

1.2 UV-Vis Absorption Spectroscopy

The experiments were carried out in air-equilibrated solutions at 25 °C. UV–Vis absorption spectra were recorded with a Perkin-Elmer Lambda 650 spectrophotometer or a Perkin-Elmer

Lambda 45 spectrophotometer using quartz cells with path length of 1.0 cm or 2.5 mL macro PMMA or UV disposable cuvettes purchased by BRAND.

1.3 Fluorescence Spectroscopy

The fluorescence spectra were recorded with a Horiba Jobin Yvon Fluoromax-4 or a Perkin-Elmer LS-55 or an Edinburgh FLS920 equipped with a photomultiplier Hamamatsu R928 phototube. The same instrument connected to a TCC900 card was used for Time Correlated Single Photon Counting (TCSPC) experiments with an LDH-P-C 405 pulsed diode laser. The fluorescence quantum yields (uncertainty, ± 15%) were determined according to the standard methods. [1]

1.4 Fluorescence Microscopy

Fluorescence microscopy was performed using an Olympus IX 71 inverted microscope equipped with a 460nm ± 10nm blue diode (LZ1-10DB00, Led-Engin) for irradiation. The microscope was connected to an ultrasensitive EMCCD Princeton PhotonMAX camera. The images were collected in time lapse mode at a rate of one image every 15 ms for a total time of 55.9 s. The blue light from the diode was focused through a converging lens on the back focus of the objective. In particular, the light was collected by a 20X or 40X objective (Olympus UPLFLN 20X or 40X) after being filtered with a band pass excitation filter (469 ± 17.5 nm, Thorlabs MF469-35) and after 90° reflection on a dichroic filter (Thorlabs MD498). The Fluorescence was filtered with a cut-off emission filter (50% transmission at 510 nm, Chroma ET510LP) to create a homogeneous light spot of 750 μm and 375 μm diameter for the 20X and 40X objectives, respectively. The irradiation intensity was managed by controlling the current intensity by a RS PRO IPS 303DD laboratory

DC power supply. The irradiance in the spot (at 0.5A, 1.0A and 1.5A) was measured with a sensor and was found to be 26.8 mW/mm^2, 47.8 mW/mm^2 and 63.1 mW/mm^2 for 20X magnification mentioned as reference intensities and 71.2 mW/mm^2, 127.2 mW/mm^2 and 168.0 mW/mm^2 for 40X magnification, mentioned as LOW, MEDIUM and HIGH intensities. For the preparation of the microscopy samples Aptaca 24x50 glass slides were used with thickness 0.13/0.17 mm. The sample was placed within two identical glass slides, which were attached to each other using double sided adhesive tape. During the irradiation, the local temperature was measured with a thermal camera Optris Xi 400 with resolution 240 μm and accuracy ±2 °C.

1.5 Dynamic Light Scattering (DLS)

DLS measurements were performed with Zetasizer Nano ZS Malvern Panalytical using PMMA semi-micro cuvettes (BRAND).

1.6 Ultra-fast Transient Absorption (UF-TA) Spectroscopy

Transient absorption (TA) experiments were carried out using a laser system, which was based on an amplified Ti:Sapphire laser that generates 100-fs pulses at 800 nm with a repetition rate of 1 kHz. The beam was initially divided through a beam splitter. One part of the beam, also called pump beam, was used to pump a non-colinear optical parametric amplifier (NOPA) to generate ~100-fs laser pulses centered at 520 nm. Pump pulses were modulated by a mechanical chopper at 500 Hz repetition rate and were delayed in time with the use of a mechanical stage. The pump was focused on a 320 μm diameter spot under a fluence of 1.5 μJ/cm^2, in order to minimize exciton-exciton annihilation processes. The other part of the beam was used to generate the probe pulses, by focusing the 800 nm beam into a thin sapphire plate, spanning from 450nm to 700nm

as detection range. The probe pulse was focused on the sample non-collinearly in respect to the pump beam on a cuvette of 1 mm path-length. The pump-probe delay time was limited up to 1 ns. The modulation of the pump pulse allowed the collection of two consecutive probe pulses, in transmission geometry, of the sample in the excited and in the ground state respectively. The UF-TA data were obtained with a magic angle (54.7°) configuration between the pump and probe polarizations. Lastly, for the analysis a global analysis algorithm (Glotaran) was used.

1.7 Transient Absorption (TA) Spectroscopy

For the Transient absorption (TA) spectroscopy, an amplified femtosecond laser (Light Conversion Pharos) was used that generated pulses of ~300 fs centered at 1024 nm, with 2 kHz repetition rate. A broadband white light probe, spanning from 480 nm till 820 nm, was generated by focusing the pulses into a thin sapphire plate. The pump light at 532 nm, with pulses of ~800 ps width, was provided by the second harmonic of a Q-switched Nd:YVO$_4$ laser (Innolas Picolo). The Q-switched Nd:YVO$_4$ laser (Innolas Picolo) was electronically triggered and synchronized to the femtosecond laser via an electronic delay. The probe pulse was focused on the sample non-collinearly with the pump beam, on a cuvette of 1 mm path-length. The TA data were obtained with a magic angle (54.7°) configuration between the pump and probe polarizations and by using a pump energy of 60 nJ per pulse. The data were collected in transmission geometry for pump-probe delay times up to 30 ns.

2. NP preparation and physicochemical characterization

2.1 NP synthesis

For the synthesis of the PDI NP, simply mentioned as NP in the main text, 2 mg of N,N'-Bis(2,5-di-tert-butylphenyl)-3,4,9,10-perylenedicarboximide (P) (CAS:83054-80-2) were diluted in 3 ml THF and were dissolved via sonication (C=0.87 mM). An 100 ml Erlenmeyer flask containing 10 ml of distilled water was placed in the sonic bath and 1ml of the perylene solution in THF prepared before was injected fast in the water (10%), while having the sonication on. The flask was sonicated until the evaporation of THF.

2.2 DLS at four Temperatures

For the DLS, the NPs were diluted 10 times in water in a PMMA semi-micro cuvette. Initially, the size of the NP was measured at 25 °C and then it was investigated in at four different Temperatures in the range of 20 to 50 °C. As it is shown in Table S1, after stabilization in each Temperature, the size of the NP was maintained always around 130 nm and was not affected by the temperature elevation.

Table S1. Z-Average and Polydispersity index values of NP at different temperatures measured by

DLS

Temperature (°C)	Polydispersity index	Z-Average
25	0.128	130.0
20	0.107	131.5
30	0.142	130.1
40	0.157	129.1
50	0.147	131.2

2.3 Quantum Yield and lifetime of NP at four different temperatures

The Quantum Yield (QY) of the NP, as well as the lifetimes, τ, at four different Temperatures are presented in table S2. The QY (uncertainty, ±15%) were determined using $[Ru(bpy)_3]^{2+}$ in water with QY = 2.8% [1].

For fitting the excited state decay acquired by TCSPC we used the following three exponential model:

$$Counts = A + B_1 e^{-\frac{t}{\tau_1}} + B_2 e^{-\frac{t}{\tau_2}} + B_3 e^{-\frac{t}{\tau_3}}$$

Table S2. Emission quantum yields and lifetimes of the NP at four temperatures

T(°C)	QY %	τ_1 (B_1) ns	τ_2 (B_2) ns	τ_3 (B_3) ns	<τ> ns
20	3.0	1.2 (35%)	4.4 (46%)	13.7 (19%)	5.0
30	2.5	1.2 (31%)	4.1 (44%)	12.7 (25%)	5.3
40	2.3	1.2 (37%)	4.1 (44%)	12.1 (19%)	4.6
50	2.1	1.1 (35%)	3.9 (47%)	11.5 (18%)	4.3

2.4 Thermal images

During irradiation of the glass slides containing the NP, the local temperature was measured with the thermal camera mentioned above and the temperature values in a 50x40 area were extracted from the thermal images for both magnifications (20X and 40X) and for all the three reference irradiation intensities, as well as the LOW, MEDIUM and HIGH intensities. As it is shown in Figure S1, the increase of the temperature of the irradiated solution was negligible and it was

within 21.2 to 21.8 ℃ with a standard deviation during each experiment that was less than 0.2

℃.
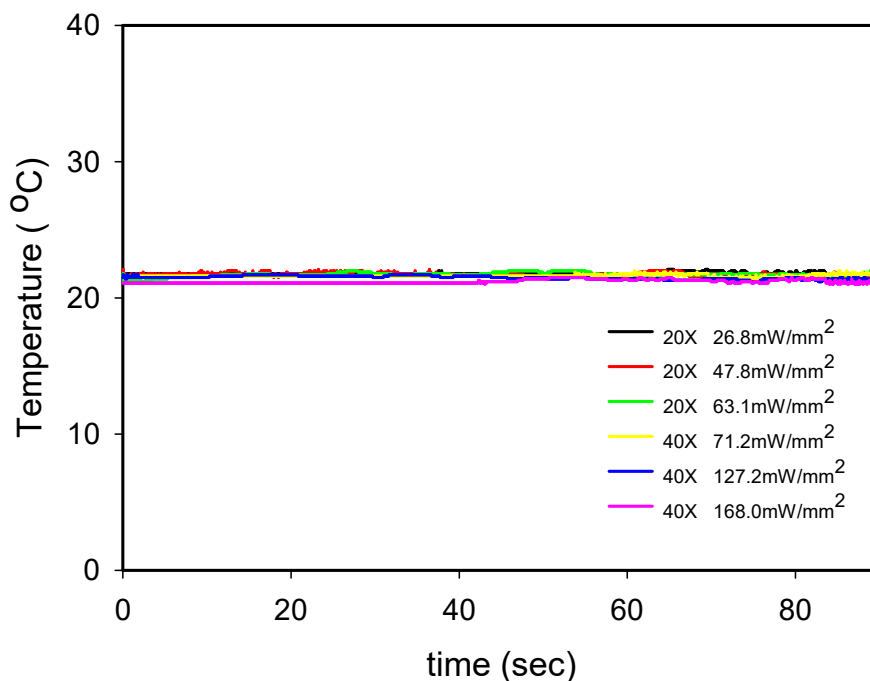
Figure S1: Temperature versus time plot of the values extracted from the thermal images during the irradiation at 20X magnification and irradiance 26.8 mW/mm², 47.8 mW/mm², 63.1 mW/mm² and 40X magnification and irradiance 71.2 mW/mm² (LOW), 127.2 mW/mm²(MEDIUM),168.0 mW/mm² (HIGH)
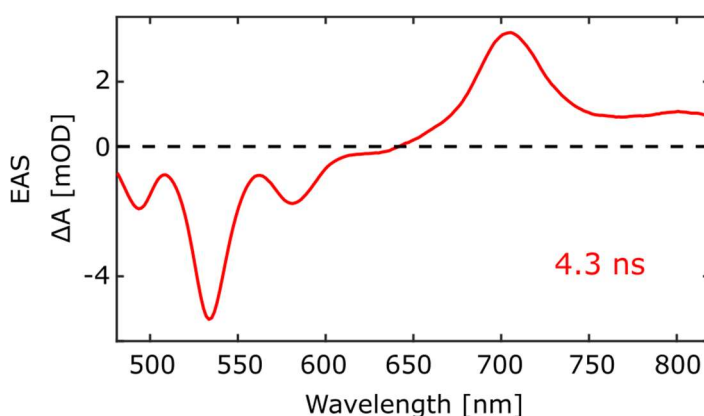
TA Spectroscopy of the P monomer

TA measurements of monomer P in DCM, after 532 nm photoexcitation are shown in Figure S2. Looking at the figure, TA spectra revealed a mirror image structure of the ground state bleach and stimulated emission components below 650 nm. Around 700 nm is prominent the characteristic S1 to Sn excited state absorption band. Moreover, in Figure S3 the evolution associated decay spectra, extracted from global kinetic analysis of the TA data of P in the same

solvent and excitation wavelength, are presented. According to the results, a relaxation of the

singlet state back to the ground state was estimated to be in 4.3 ns.
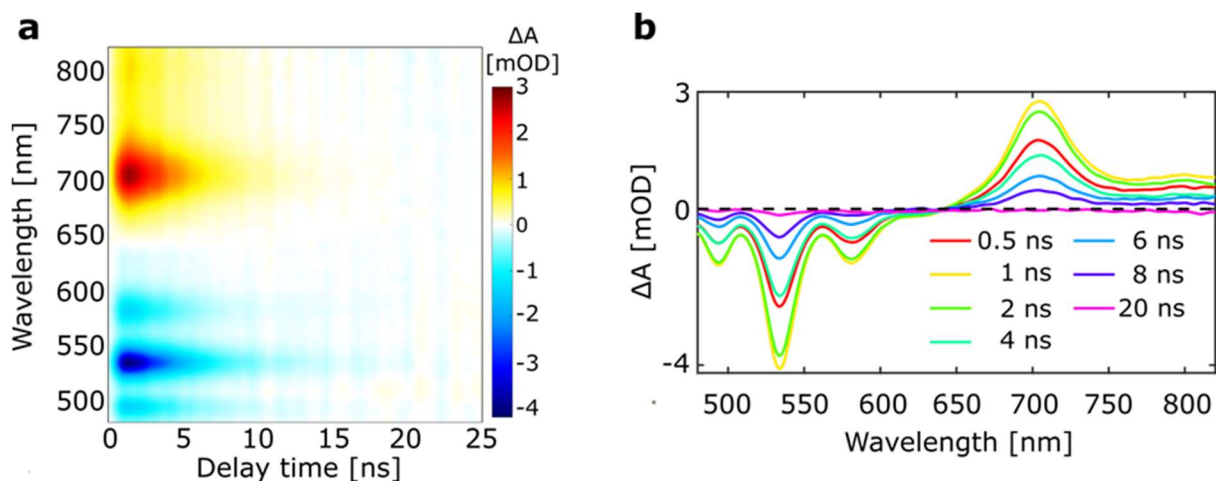
Figure S2. Transient absorption (TA) spectroscopy of P monomer in DCM after 532 nm photoexcitation; (a) TA map for detection wavelengths ranging from 480 nm till 820 nm collected till 25 ns; (b) Differential absorption cuts of the TA map for specific pump probe delay times.
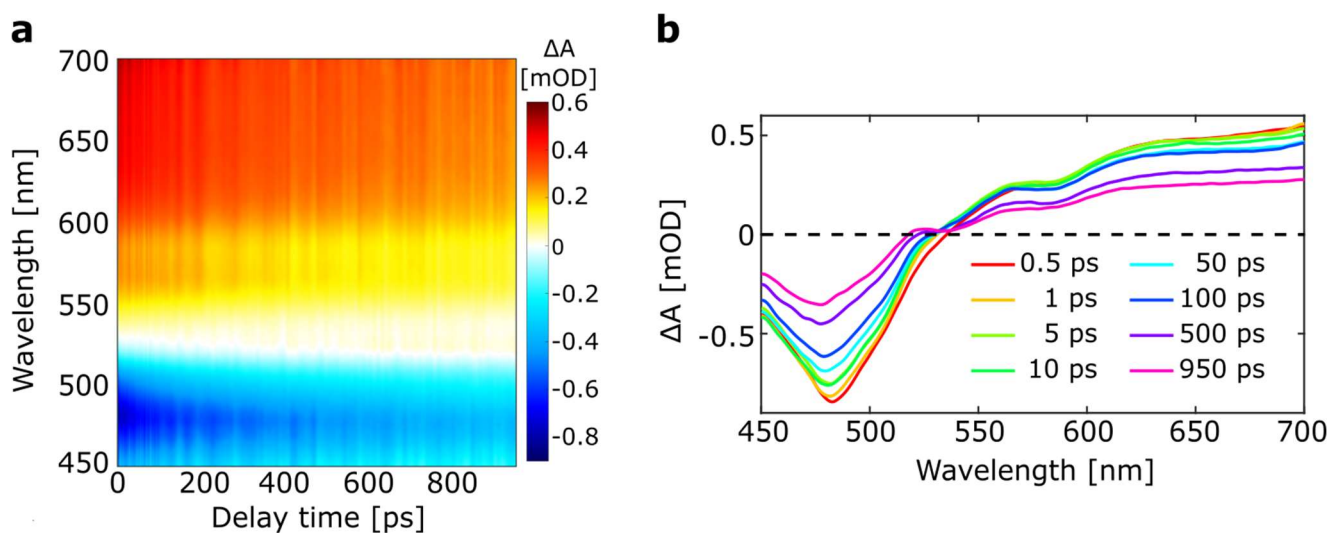

Figure S3. Evolution associated decay spectra extracted from global kinetic analysis of the TA data of P after excitation at 532 nm.

2.5 UF-TA Spectroscopy of the NP

Th UF-TA signals of the NP in water after excitation at 520 nm photoexcitation are shown in Figure S4, while evolution associated decay spectra extracted from global kinetic analysis of the UF-TA data of NP after excitation at 520 nm are illustrated in Figure S5. Right after excitation, the spectral signatures of PDI radical cation (570 nm), PDI radical anion (620 nm) and the PDI local excited state (700 nm) are present. The mixed Frenkel and CT states decay into a CT resonance excimer state within 1.4 ps, in line with the spectral growth at 570 nm. The CT resonance excimer undergoes structural relaxation within 140 ps, in accordance with the unchanged shape of the excited state absorption spectrum. The CT resonance excimer decays back to the ground state in a timescale longer than the pump-probe delay time available by our apparatus (> 1 ns).

Figure S4. Ultrafast transient absorption (UF-TA) spectroscopy of PDI Nanoparticles (NP) in water after 520 nm photoexcitation; (a) UF-TA map for visible range detection spanning from 450 nm till 700 nm, recorded till 1 ns pump probe delay time; (b) Differential absorption cuts of the UF-TA map for specific pump probe delay times.
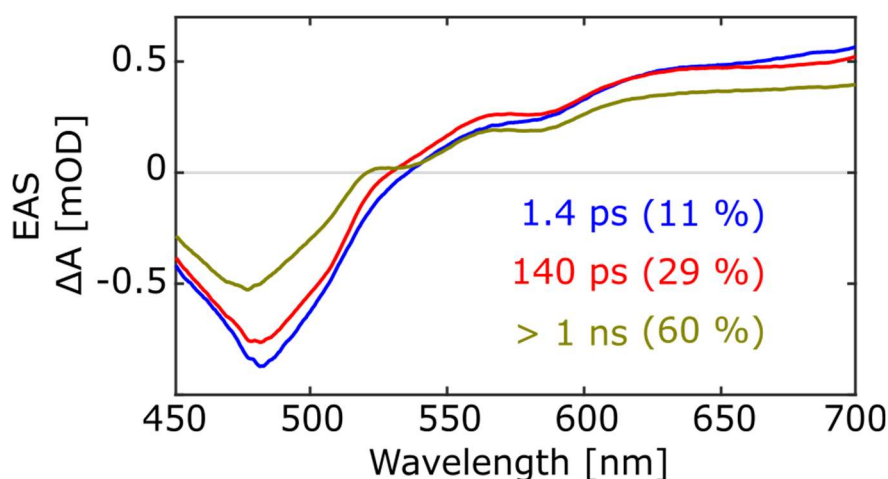
Figure S5. Evolution associated decay spectra extracted from global kinetic analysis of the UF-TA data of NP after excitation at 520 nm

2.6 Estimation of the adsorbed and dissipated energy

An estimation of the energy losses of the system that is dissipated as a heat, can be done through the recovery of the ground state bleaching signal and/or through the non-radiative relaxation to a lower electronic state. After excitation of the upper allowed state, the system relaxes to the lowest electronic state of the CT resonance excimer within 1.4 ps. In the spectral region above 520 nm, there is an interplay between the populations of the Frenkel excitons, CT states and CT resonance excimer during this process. In contrast, in the spectral region of 450 nm till 520 nm there is prominent only the ground state bleaching signal. Thus, we calculate through the recovery of the ground state (integral area from 450 nm till 520 nm) a percentage of at least 11% which is dissipated within the timescale of this process. Afterwards, the CT resonance excimer undergoes structural relaxation within 140 ps. As a relaxation process is not altering the overall

proportions of the contributed excited state species (unchanged ESA shape), we calculate through the decay of the integrated area underneath the whole spectra (from 450 nm till 700 nm) an additional 29% of energy dissipated. The rest 60% decays back to the ground state in a timescale longer than the pump probe delay time available by our apparatus UF-TA system (> 1 ns). Time-resolved fluorescence spectroscopy and emission quantum yield calculations, allow us to estimate that within a mean lifetime of 5 ns, only the 3% of the excited energy is lost through radiative processes while the rest 57% is dissipated as heat.

In a steady state irradiation regime of the tracking experiments a section of surface S (mm²) is homogeneously irradiated with a perpendicular light beam of irradiance p/S (W/mm²).

The solution layer has thickness d(cm) and its concentration is c(M) of NP/molecules with molar absorption coefficient ε(M⁻¹cm⁻¹). A is the absorbance measured for the film.

Considering a total power p integrated on the surface S, the number of photon at wavelength λ is calculated by:

$$F_0 = p\,\lambda\,5.03\,10^{15}$$

Only a part of these photons is absorbed by the NP and in particular according to Lambert-Beer's law;

$$\frac{F_{ass}}{F_0} = 1 - 10^{-\varepsilon}$$

Where c is mol/L and d is in cm. For low absorbance:

$$\frac{F_{ass}}{F_0} = 2.3\varepsilon cd$$

Hence, the total number of absorbed photons is:

$$F_{ass} = p\,\lambda\,5.03\ 10^{15}2.3\varepsilon cd$$

On the other hand, the number of particles n in the Sd volume (where S is mm² and d in cm) is:

$$n = 10^{-5}cNSd$$

Hence, the average number of photon adsorbed per NP per second is:

$$\frac{F_{ass}}{n} = \frac{1}{10^{-5}cNSd}p\,\lambda\,5.03\ 10^{15}2.3\varepsilon cd$$

And simplifying

$$\frac{F_{ass}}{n} = \frac{1}{10^{-5}N}\frac{p}{S}\lambda\,5.03\ 10^{15}2.3\varepsilon$$

Assuming $\lambda = 460\ nm$

$$\frac{F_{ass}}{n} = \frac{1}{10^{-5}N}\frac{p}{S}\lambda\,5.03\ 10^{15}2.3\varepsilon$$

And hence:

$$\frac{F_{ass}}{n} = 0.884\frac{p}{S}\varepsilon$$

Where p/S is 71.2 mW/mm², 127.2 mW/mm² and 168.0 mW/mm² at LOW, MEDIUM and HIGH regime respectively and $1.55\text{x}10^{10}$ M^{-1} cm^{-1} for the NP.

A similar expression can be obtained for the absorbed energy

$$\frac{p_{ass}}{n} = \frac{F_{ass}}{n}\frac{1}{\lambda\,5.03\ 10^{15}}$$

2.7 Calculation of the photothermal conversion efficiency

The total energy balance of the system can be expressed as:

$$\sum_i m_i C_{Pi} \frac{dT}{dt} = Q_{NP} + Q_D - Q_s$$

Where m and C_p are respectively the mass and heat capacity of water, T the solution temperature, Q_{NP} is the energy inputted by NP, Q_D the baseline energy inputted by sample cell and finally Q_s is heat conducted away from the system surface by air.

The light-induced term, Q_{NP}, represents the heat dissipated by radiationless relaxation of PBI NPs excited states under the irradiation of 460nm LED:

$$Q_{NP} = I(1 - 10^{-A460})\eta$$

Where I is the irradiation light power, η is the conversion efficiency from radiative energy to thermal energy, and A_{460} is PBI NP absorbance at wavelength 460 nm. In addition, Q_D source term expresses the heat dissipated from light absorbed by sample cell containing pure water.

Finally, Qs is given by the linear equation:

$$Q_S = hS(T - T_S)$$

Where h is the heat transfer coefficient, S is the surface area of sample cell and T_S is the ambient temperature of surroundings. For a defined irradiation power, the system heat input, $(Q_{NP} + Q_D)$ resulted to be finite. Since the heat output (Qs) increases linearly with temperature, the resulting system temperature will reach a maximum when the heat input and output are equal:

$$Q_{NP} + Q_D = Q_{s\,max} = hS(T_{max} - T_S)$$

Where $Q_{s\,max}$ is heat conducted away from the system surface by air at equilibrium temperature and T_{max} the equilibrium temperature. Heat conversion efficiency (η) can be determined rearranging former equations to get:

$$\eta = \frac{hS(T_{max} - T_S) - Q_D}{I(1 - 10^{-A46})}$$

Where Q_D was measured to be 0.01 Js^{-1}, $(T_{max} - T_S)$ was 10.3 °C, $I(1 - 10^{-A460})$ was 0.28 Js^{-1}. In order to get hS, a dimensionless driving force temperature θ is introduced:

$$\theta = \frac{T - T_S}{T_{max} - T_S}$$

And a sample system time constant τ_s expressed as:

$$\tau_s = \frac{\sum_i m_i C_{Pi}}{hS}$$

Which is substituted and rearranged in

$$\frac{d\theta}{dt} = \frac{1}{\tau_s}\left[\frac{Q_{NP} + Q_D}{hS(T_{max} - T_S)} - \theta\right]$$

At cooling stage of the solution, the LED was shut off, the $Q_{NP} + Q_D = 0$, reducing

$$dt = -\tau_s ln\theta$$

And integrating, giving the expression:

$$t = -\tau_s ln\theta$$

Therefore, time constant for heat transfer from the system is determined to be $\tau_s = 466$ s. In addition, m is 3.0 g and the C is 4.18 Jg^{-1}K^{-1}. Thus, the hS is deduced to be 0.027 W/°C and the photothermal conversion efficiency $\eta = 95\%$

3. Results interpretation

3.1 Calculation of the number of P molecule per NP and NP concentration.

The number of P molecule per NP was estimated by considering the molar volume of the NP:

$$V = N\frac{4}{3}\pi R^3$$

Where N is the Avogadro number R is the radius of the NP. In order to obtain the volume in dm3

R should be expressed in dm=108nm. Hence if R is in nm:

$$V = 6.02\ 10^{23}\frac{4}{3}R^3\pi 10^{-24}$$

$$V = 2.52\ R^3$$

For R=65 nm V=6.92 105 dm³. Considering the molar volume of P (MW=766.96 g/mol) 0.766 dm³

The number of P per NP are 9.0x105. NP are prepared from solution 0.67 mg/ml diluted 1 to 10

hence concentration is 0.087 mM of P and 9.7 x 10^{-11} M of NP. After 1 to 10 dilution is 9.7 x 10^{-12}

M.

3.3 Analysis of the trajectories

3.3.1 Extraction of the trajectories from the movies

In this part, the three reference intensities at 20X magnification, 26.8 mW/mm², 47.8 mW/mm², 63.1 mW/mm², are going to be mentioned as A1, A2, A3, while the LOW, MEDIUM and HIGH intensities, 71.2 mW/mm², 127.2 mW/mm²,168.0 mW/mm², are going to be mentioned as B1, B2 and B3 respectively. Time lapsed image sequences A1, A2, A3 and B1, B2, B3 were recorded as *.SPE files (16-bit depth) opened with Image-J. The plug-in Mosaic was used for NP position and trajectory identification (3, 0.25, 0.3, 1 ,5).

The resulting trajectories were saved as text files: A1.TXT, A2.TXT, A3.TXT, B1.TXT, B2.TXT and B3.TXT.

These files were hence imported in Sigmaplot in a worksheet starting form cell(1,1) giving in col(1) a progressive index n for each coordinate pair (X, Y) where the coordinate X is placed in col(4) and coordinate Y is placed in col(5). In col(2) an index that identify one specific trajectory i and in col(3) the number of the frame t where the (X, Y) was identified.

3.3.2 Calculation of the displacements

After processing the data with the following a set of commands:

```
s=1
for n=1 to 100000 do
cell(6,n)=cell(2,n*s+1)-cell(2,(n-1)*s+1)
cell(7,n)=cell(4,n*s+1)-cell(4,(n-1)*s+1)
cell(8,n)=cell(5,n*s+1)-cell(5,(n-1)*s+1)
```

end for

col(9)=col(3)

col(10)=sqrt(col(7)^2+col(8)^2)

in col(7) were reported all the displacements ΔX, and in col(8) the respective displacements ΔY. In col(8) was reported the linear bidimensional displacement. Only in the case in which the value in col(6) is 0 the calculated displacements correspond to the same NP and hence are real displacements. Hence all the lines having col(6)=1 were eliminated.

3.3.3 Averaging of the bidimensional displacement

In order to follow the evolution of the mono- e bidimensional displacement during time (hence in the sequence) the data were ordered for increasing values of time (t) which is both in col(3) and col(9).

Hence, in order to follow the average displacement during the running average of col(9) and col(10) over 500 data points was calculated.

col(9)=runavg(col(9),500)

col(10)=runavg(col(10),500)

The average displacement as a function of time was hence plotted.

3.3.4 Fitting of the unidimensional displacement

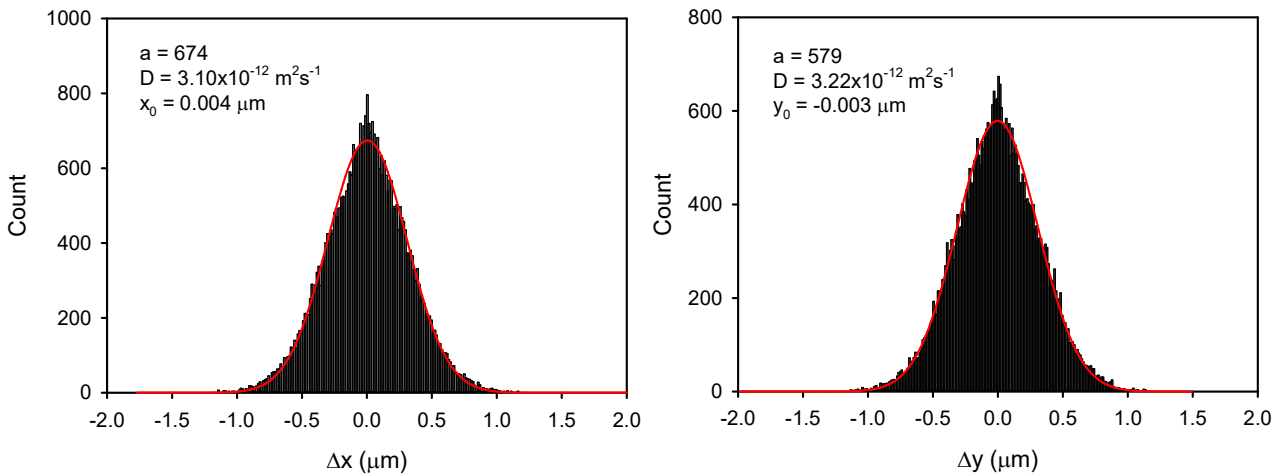In order to estimate the overall diffusion coefficients in the X and Y direction the displacements ΔX and ΔY (col(7) and col(8)) respectively were plotted in a histogram (binning=300) and fitted
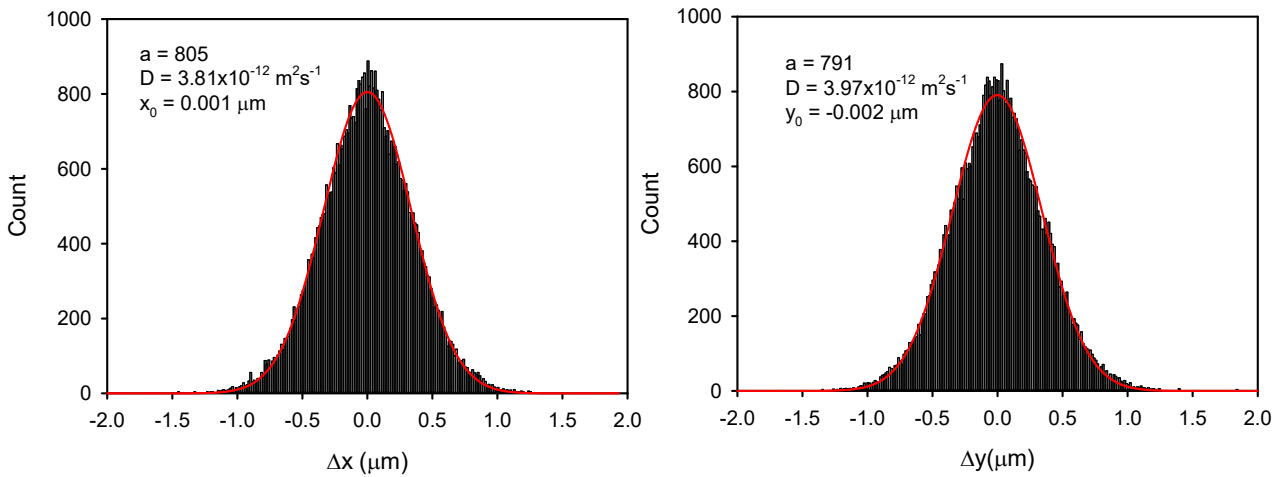
with a Gaussian peak (3 parameters) as expected for brownian diffusion according to the

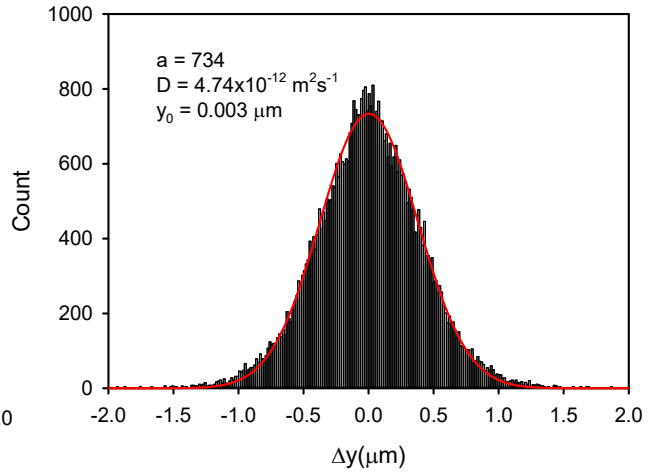function:

$$f = a*exp(-((\Delta x - x_0)^2 / 4D\Delta t)$$

I1 intensity (71.2 mW/mm²)

a = 674
$D = 3.10 \times 10^{-12}$ m²s⁻¹
$x_0 = 0.004$ µm

a = 579
$D = 3.22 \times 10^{-12}$ m²s⁻¹
$y_0 = -0.003$ µm

I2 intensity (127.2 mW/mm²)

a = 805
$D = 3.81 \times 10^{-12}$ m²s⁻¹
$x_0 = 0.001$ µm

a = 791
$D = 3.97 \times 10^{-12}$ m²s⁻¹
$y_0 = -0.002$ µm

I3 intensity (168.0 mW/mm²)

a = 741
D = 4.61x10^{-12} m^{2}s^{-1}
x$_0$ = -0.004 µm
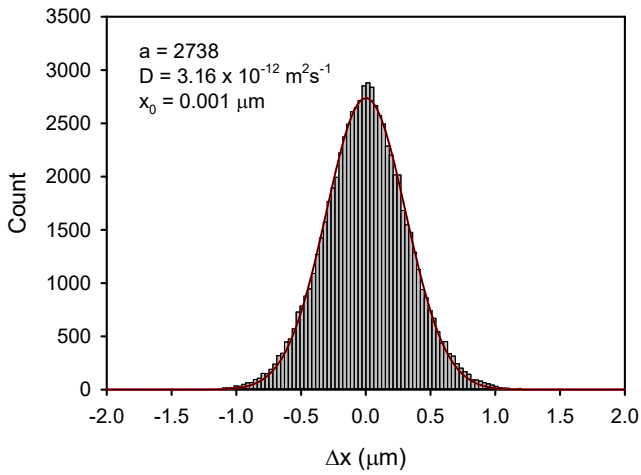
a = 734
D = 4.74x10^{-12} m^{2}s^{-1}
y$_0$ = 0.003 µm

IRRADIANCE 26.8 mW/mm^2

a = 2738
D = 3.16 x 10^{-12} m^{2}s^{-1}
x$_0$ = 0.001 µm

a = 2548
D = 3.08 x 10^{-12} m^{2}s^{-1}
y$_0$ = -0.005 µm

IRRADIANCE 47.8 mW/mm^2

a = 2740
D = 3.18x10^{-12} m^{2}s^{-1}
x$_0$ = 0.001µm
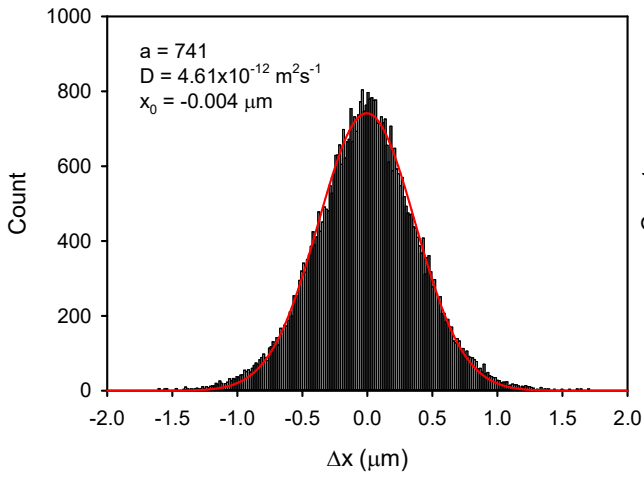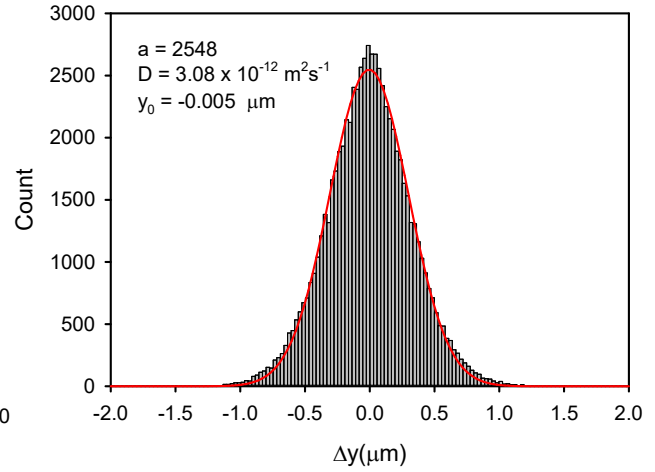
a = 2130
D = 3.14x10^{-12} m^{2}s^{-1}
y$_0$ = -0.002
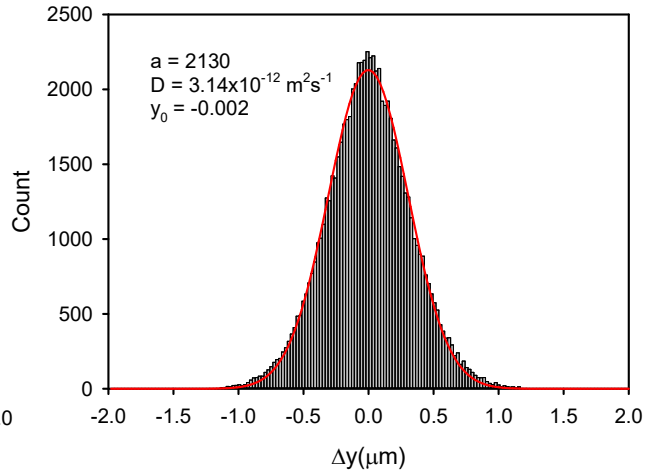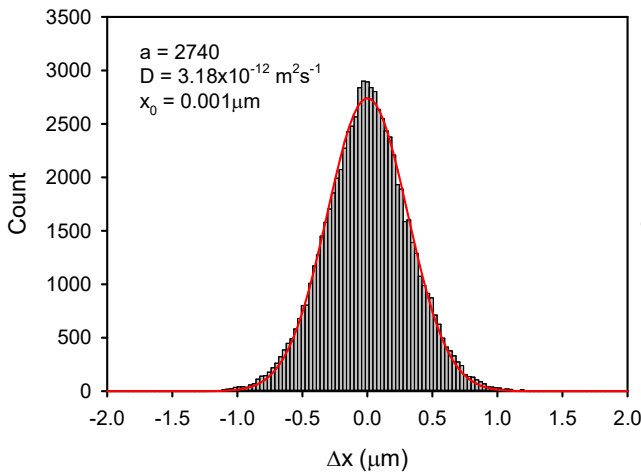
IRRADIANCE 63.1 mW/mm^2
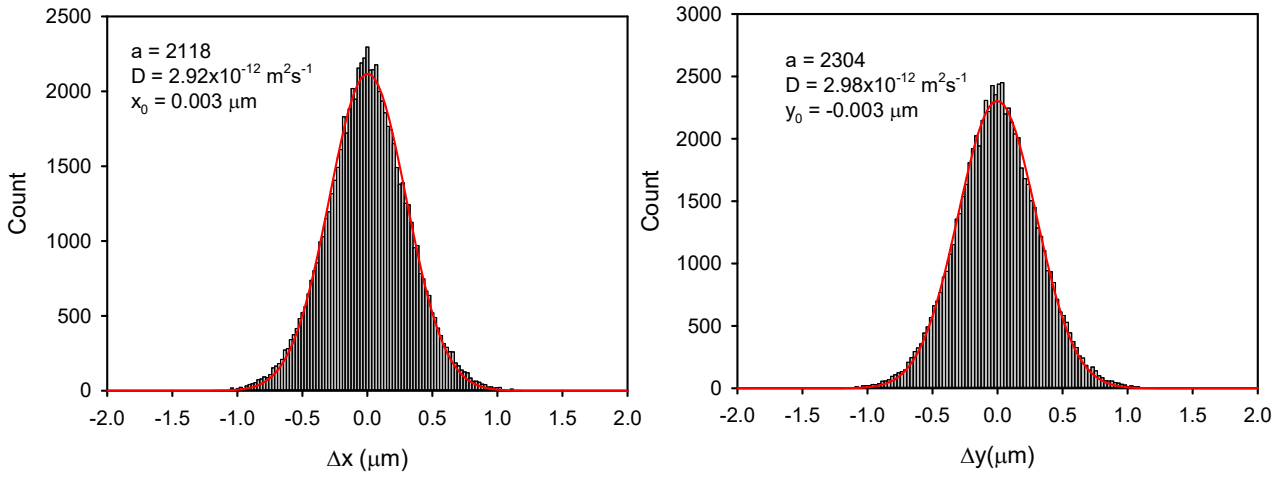
3.4 Anomalous diffusion object analysis (ADOMA)

For the investigation of the diffusion process in detail, the ten longest trajectories for all the three LOW, MEDIUM and HIGH intensities were chosen and analyzed. In particular, Anomalous diffusion object analysis (ADOMA) was used to provide information about the motion [2][3][4] of the NP upon increasing irradiance (71.2, 127.2 and 168.0 mW/mm²). It uses the various moments, q, of the displacement, r, according to the equation:

Eq. S1
$$< |r|^q > (\tau) = \frac{1}{T-\tau} \sum_{n=1}^{T-\tau} |r(n+\tau) - r(n)|^q \propto \tau^{z(q)}$$

where q is the order of the moment taking values in the range [0.25,3] with step of 0.25, τ is the time lag defined in statistical sense, the used value of the observed quantity at time τ is the mean average over all events separated by time τ along the trajectory of length T-τ, $z(q)$ is the structure function and its value for each moment is obtained by linear regression of eq. S1. If $z(q) = Hq$ then the process is monofractal [5][6][7]. If $z(q)$ is a bilinear function of q then the stochastic process is either as Levy walks or as Levy flights. If $z(q)$ has convex shape then the process is multifractal. [4][8][9] The trajectories were analyzed by means of eq.(S1) as it shown in Figure S6 and Tables S3, S4 and S5. In all the cases, $z(q)$ is a linear function of q revealing that the underlying stochastic process is monofractal.
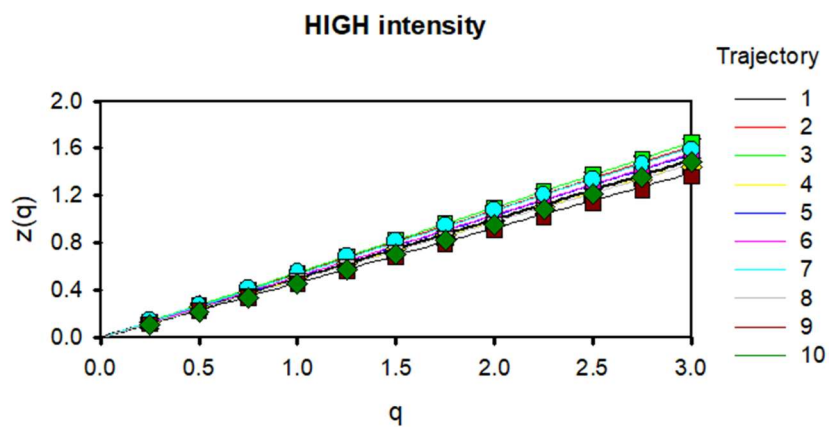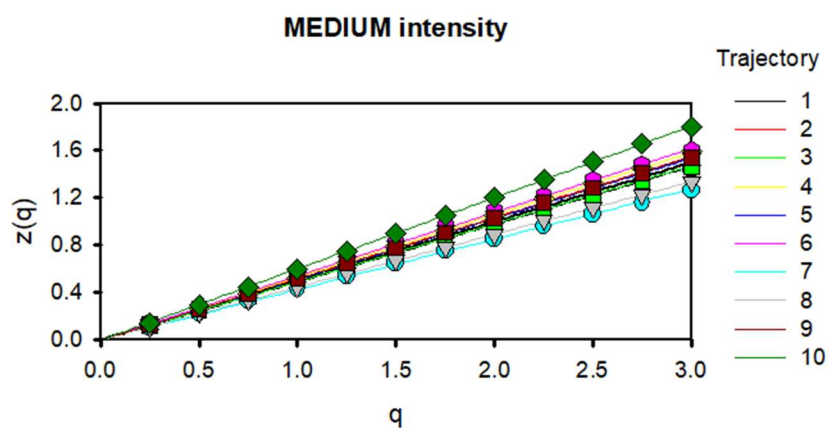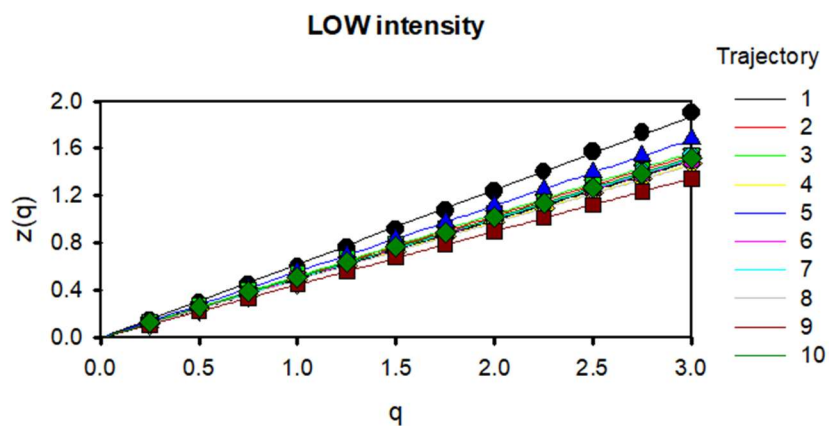
Figure S6: The structure functions z(q) of the ten longest trajectories for LOW, MEDIUM and HIGH irradiation intensities
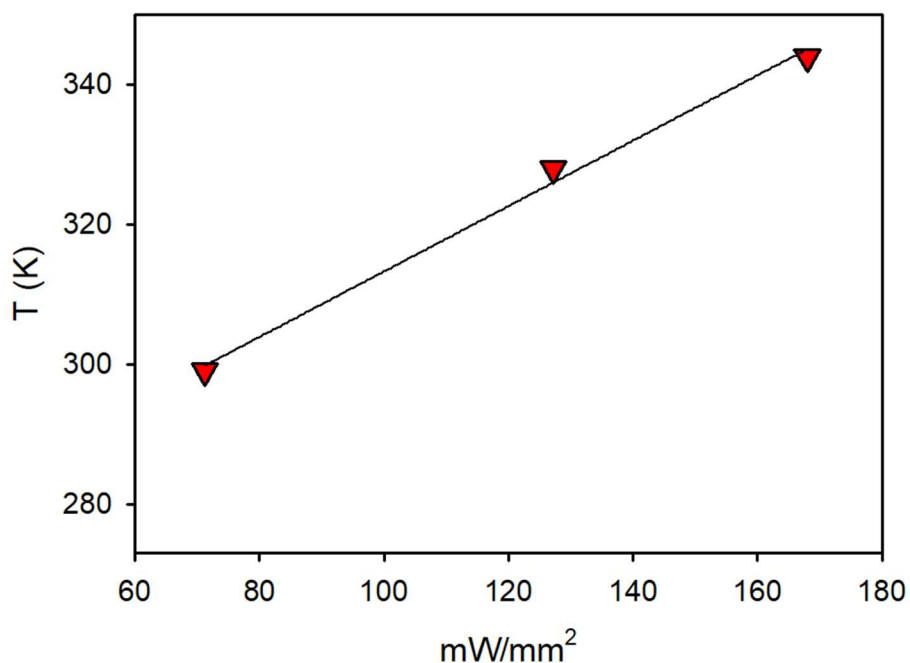
Figure S7: Effective Temperature to irradiation intensity plot and linear fitting for the LOW, MEDIUM and HIGH irradiation intensities

Table S3. LOW intensity (71.2 mW/mm²) : Hurst exponent (H) of the structure function z(q)=Hq, scaling exponent (γ), Diffusion coefficient (D), and Temperature (T_{eff}) for each one of the ten analyzed trajectories. The ensemble average values for γ, D_0, and T are 1, 3.22x10⁻¹² m²/sec, and 299 K.

Progressive numbering	H	γ	D(10-12 m²/sec)	T_{eff}(K)
1	0.625±0.003	1.240±0.006	6.680	620.977
2	0.516±0.001	1.029±0.011	3.155	293.291
3	0.522±0.002	1.052±0.011	2.724	253.225
4	0.489±0.001	0.977±0.018	2.782	258.616

5	0.559±0.001	1.117±0.005	4.741	440.726
6	0.503±0.001	1.010±0.018	2.804	260.662
7	0.504±0.002	1.002±0.008	2.910	270.515
8	0.487±0.004	0.957±0.012	1.677	155.895
9	0.450±0.0004	0.902±0.015	1.621	150.689
10	0.508±0.001	1.019±0.015	3.093	287.527

Table S4. MEDIUM intensity (127.2 mW/mm^2) : Hurst exponent (H) of the structure function z(q)=Hq, scaling exponent (γ), Diffusion coefficient (D), and Temperature (Teff) for each one of the ten analyzed trajectories. The ensemble average values for γ, D_0, and T are 1, 3.53×10^{-12} m^2/sec, and 328 K.

Progressive numbering	H	γ	D(10-12 m2/sec)	Teff(K)
1	0.488±0.002	0.985±0.015	3.439	319.692
2	0.517±0.002	1.045±0.011	3.988	370.727
3	0.491±0.001	0.984±0.010	3.311	307.793
4	0.529±0.001	1.058±0.004	4.320	401.590
5	0.512±0.002	1.031±0.006	2.827	262.800
6	0.540±0.002	1.087±0.005	4.550	422.971
7	0.426±0.001	0.857±0.017	2.117	196.798
8	0.446±0.001	0.895±0.013	2.599	241.605
9	0.515±0.001	1.034±0.008	2.838	263.822
10	0.602±0.001	1.208±0.003	5.334	495.852

Table S5. HIGH_intensity (168.0 mW/mm²): Hurst exponent (H) of the structure function $z(q)=Hq$, scaling exponent (γ), Diffusion coefficient (D), and Temperature (Teff) for each one of the ten analyzed trajectories. The ensemble average values for γ, D_0, and T are 1, 3.70×10^{-12} m²/sec, and 344 K.

Progressive numbering	H	γ	D(10^{-12} m²/sec)	Teff(K)
1	0.464±0.002	0.919±0.020	3.374	313.649
2	0.540±0.002	1.074±0.004	5.135	477.353
3	0.550±0.001	1.102±0.005	4.146	385.415
4	0.490±0.003	0.990±0.009	3.200	297.474
5	0.516±0.002	1.028±0.008	4.064	377.792
6	0.519±0.003	1.045±0.004	3.261	303.145
7	0.536±0.002	1.078±0.009	4.856	451.417
8	0.489±0.001	0.983±0.008	2.919	271.352
9	0.455±0,001	0.908±0.011	2.186	203.212
10	0.484±0,001	0.956±0.013	3.900	362.546

The scaling exponent for ensemble average shows to Brownian motion and thus the diffusion coefficient D_0 can be used for the estimate of the system temperature through the first dissipation fluctuation theorem (FDFT), known also as Stokes-Einstein equation, according to the equation:

$$\text{Eq. S2} \qquad\qquad D_0 = \frac{k_B T}{6\pi\eta R}$$

where k_B is the Boltzmann's constant, T is the absolute temperature, η is the viscosity of the environment, taken equal to 0.001 Pa s, and R~65 nm is the radius of the diffusing molecule.

The probabilities, $P(\xi)$, were also well-fitted to the gamma distribution, $f(\xi, r, \beta) = c\frac{r(r\xi)^{\beta-1}}{\Gamma(\beta)}e^{-r}$, where β is the shape parameter, r is the rate parameter and c is a weighting factor,

all their values are listed in Table S6. Gamma distributions arise in the presence of diffusivity that changes locally. [10] [11] [12]

Table S6. Fitting parameters for the probability distribution of the random variable $P(\xi)$ versus ξ, where $\xi = \frac{l}{<l>}$. The values of $P(\xi)$ fit well the gamma distribution, $f(\xi, r, \beta) = c\frac{r^{\beta}\xi^{\beta-1}}{\Gamma(\beta)}e^{-r}$, where β is the shape parameter, r is the rate parameter and c is a weighting factor. The data and the best fittings are shown in Figure 6 of the main text.

a/a	LOW			MEDIUM			HIGH		
	c	r	β	c	r	β	c	r	β
1	0.551± 0.005	3.908± 0.086	5.067± 0.094	0.524± 0.004	3.776± 0.073	4.919± 0.080	0.564± 0.024	3.381± 0.344	4.463± 0.382
2	0.561± 0.012	3.693± 0.201	4.752± 0.222	0.566± 0.003	4.093± 0.057	5.221± 0.062	0.542± 0.019	3.363± 0.286	4.371± 0.315
3	0.579± 0.027	2.887± 0.368	3.821± 0.416	0.521± 0.022	3.456± 0.356	4.539± 0.102	0.537± 0.002	4.318± 0.046	5.488± 0.050
4	0.521± 0.029	3.479± 0.448	4.562± 0.495	0.512± 0.005	4.210± 0.092	5.407± 0.102	0.545± 0.016	4.140± 0.276	5.259± 0.298
5	0.519± 0.004	3.932± 0.074	5.061± 0.081	0.545± 0.023	3.507± 0.345	4.672± 0.387	0.550± 0.019	3.297± 0.293	4.340± 0.325
6	0.523± 0.026	3.770± 0.434	4.943± 0.486	0.520± 0.011	4.029± 0.194	5.172± 0.213	0.572± 0.016	3.523± 0.247	4.633± 0.276
7	0.493± 0.011	4.086± 0.222	5.291± 0.247	0.537± 0.015	4.029± 0.280	5.156± 0.307	0.513± 0.024	4.015± 0.400	5.210± 0.446
8	0.529± 0.013	3.983± 0.222	5.172± 0.246	0.538± 0.030	3.751± 0.495	4.923± 0.554	0.565± 0.003	3.668± 0.042	4.696± 0.046
9	0.544± 0.006	4.039± 0.104	5.172± 0.113	0.568± 0.027	2.710± 0.322	3.632± 0.357	0.525± 0.049	3.771± 0.786	5.042± 0.898

10	0.552± 0.008	3.668± 0.134	4.776± 0.149	0.546± 0.007	4.528± 0.138	5.726± 0.149	0.545± 0.013	3.673± 0.210	4.778± 0.230

4. References

1.	Montalti, M.; Credi, A.; Prodi, L.; Gandolfi, M. T.; Michl, J.; Balzani, V., *Handbook of photochemistry*. 2020.

2.	Parent, L. R.; Bakalis, E.; Ramírez-Hernández, A.; Kammeyer, J. K.; Park, C.; de Pablo, J.; Zerbetto, F.; Patterson, J. P.; Gianneschi, N. C., Directly Observing Micelle Fusion and Growth in Solution by Liquid-Cell Transmission Electron Microscopy. *Journal of the American Chemical Society* **2017,** *139* (47), 17140-17151.

3.	Parent, L. R.; Bakalis, E.; Proetto, M.; Li, Y.; Park, C.; Zerbetto, F.; Gianneschi, N. C., Tackling the Challenges of Dynamic Experiments Using Liquid-Cell Transmission Electron Microscopy. *Accounts of Chemical Research* **2018,** *51* (1), 3-11.

4.	Bakalis, E.; Parent, L. R.; Vratsanos, M.; Park, C.; Gianneschi, N. C.; Zerbetto, F., Complex Nanoparticle Diffusional Motion in Liquid-Cell Transmission Electron Microscopy. *The Journal of Physical Chemistry C* **2020,** *124* (27), 14881-14890.

5.	Bakalis, E.; Höfinger, S.; Venturini, A.; Zerbetto, F., Crossover of two power laws in the anomalous diffusion of a two lipid membrane. *The Journal of Chemical Physics* **2015,** *142* (21), 215102.

6.	Giangreco, F.; Höfinger, S.; Bakalis, E.; Zerbetto, F., Impact of the green tea ingredient epigallocatechin gallate and a short pentapeptide (Ile-Ile-Ala-Glu-Lys) on the structural organization of mixed micelles and the related uptake of cholesterol. *Biochimica et Biophysica Acta (BBA) - General Subjects* **2018,** *1862* (9), 1956-1963.

7.	Sändig, N.; Bakalis, E.; Zerbetto, F., Stochastic analysis of movements on surfaces: The case of C60 on Au(111). *Chemical Physics Letters* **2015,** *633*, 163-168.

8.	Devaux, F.; Li, X.; Sluysmans, D.; Maurizot, V.; Bakalis, E.; Zerbetto, F.; Huc, I.; Duwez, A.-S., Single-molecule mechanics of synthetic aromatic amide helices: Ultrafast and robust non-dissipative winding. *Chem* **2021,** *7* (5), 1333-1346.

9.	Bakalis, E.; Mertzimekis, T. J.; Nomikou, P.; Zerbetto, F., Breathing modes of Kolumbo submarine volcano (Santorini, Greece). *Scientific Reports* **2017,** *7* (1), 46515.

10.	Hapca, S.; Crawford, J. W.; Young, I. M., Anomalous diffusion of heterogeneous populations characterized by normal diffusion at the individual level. *Journal of The Royal Society Interface* **2009,** *6* (30), 111-122.

11.	Postnikov, E. B.; Chechkin, A.; Sokolov, I. M., Brownian yet non-Gaussian diffusion in heterogeneous media: from superstatistics to homogenization. *New Journal of Physics* **2020,** *22* (6), 063046.

12.	Wang, W.; Cherstvy, A. G.; Chechkin, A. V.; Thapa, S.; Seno, F.; Liu, X.; Metzler, R., Fractional Brownian motion with random diffusivity: emerging residual nonergodicity below the correlation time. *Journal of Physics A: Mathematical and Theoretical* **2020,** *53* (47), 474001.